

Article

# In-Situ Growth of Au on $\text{KTaO}_3$ Sub-Micron Cubes via Wet Chemical Approach for Enhanced Photodegradation of p-Nitrophenol

Shengding Chang<sup>1</sup>, Muwei Ji<sup>1,2</sup>, Changxu Yan<sup>1</sup>, Kai Zhang<sup>1</sup>, Qian Deng<sup>1</sup>, Jian Xu<sup>2</sup>, Caizhen Zhu<sup>2</sup>, Bo Li<sup>1</sup> and Jin Wang<sup>1,\*</sup>

<sup>1</sup> Graduate School at Shenzhen, Tsinghua University, Shenzhen 518055, China; csd16@mails.tsinghua.edu.cn (S.C.); jimwei@163.com (M.J.); ycx17@mails.tsinghua.edu.cn (C.Y.); zhangkai17@mails.tsinghua.edu.cn (K.Z.); dq17@mails.tsinghua.edu.cn (Q.D.); boli@mail.tsinghua.edu.cn (B.L.)

<sup>2</sup> Institute of Low-dimensional Materials Genome Initiative, College of chemistry and environmental engineering, Shenzhen University, Shenzhen 518060, China; jxu@iccas.ac.cn (J.X.); makingway@163.com (C.Z.)

\* Correspondence: wang.jin@sz.tsinghua.edu.cn

Received: 30 April 2019; Accepted: 14 June 2019; Published: 17 June 2019



**Abstract:**  $\text{KTaO}_3/\text{Au}$  hetero-nanostructures were synthesized by in-situ reduction of  $\text{HAuCl}_4$  on the surface of hydrothermally-grown  $\text{KTaO}_3$  sub-micron cubes. The concentration of Au source was found to be a critical factor in controlling the hetero-nucleation of Au nanoparticles on the surface of  $\text{KTaO}_3$  sub-micron cubes. Loading of Au particles on  $\text{KTaO}_3$  nanocrystals enriched  $\text{KTaO}_3$  additional UV-vis absorption in the visible light region. Both  $\text{KTaO}_3$  and  $\text{KTaO}_3/\text{Au}$  nanocrystals were shown to be active in the photo-degradation of p-nitrophenol, while the loading of Au on  $\text{KTaO}_3$  clearly improved the photo-degradation efficiency of p-nitrophenol compared to that on bare  $\text{KTaO}_3$  nanocrystals, probably due to the improved light absorption and charge separation.

**Keywords:** in-situ synthesis;  $\text{KTaO}_3/\text{Au}$  hetero-nanostructures; concentration of Au source; photo-degradation of p-nitrophenol

## 1. Introduction

Potassium tantalates and their derivatives are wide-band gap semiconductors that are extensively applied in many fields, including gas phase condensation, photo-transporting, photo-detector, air-treatment, photo-conducting and photo-electronic response [1–6]. Furthermore, potassium tantalates are considered one kind of the most stable photoelectric catalysts and are widely employed in photonically-driven  $\text{CO}_2$  reduction [7,8], water splitting and hydrogen evolution [7–10]. While potassium tantalates exhibit excellent stability in photocatalysis, their absorption locates at Ultra-violet (UV) range and limits the employment of visible light. In order to make use of solar energy with higher efficiency, various methods are explored to modify potassium tantalates, such as cations doping [11,12] and construction of hetero-structure [13,14]. For instance, porphyrin was used as mixing dyes to sensitize potassium tantalates for photo-splitting water to  $\text{H}_2$  or  $\text{O}_2$  [8]. Design and construction of hetero-structure is a facile method to enhance the light absorption and facilitate the charge separation [9,15–17]. Au nanoparticles were known as an effective enhancer on photocatalysis due to the charge-separation effect and their plasmonic effects [18]. Moreover, the Au nanoparticles were reported that their plasma enhancement depends on their sizes and morphologies [19–22]. Hence, controlled growth of Au nanoparticles on  $\text{KTaO}_3$  nanocrystals is a

possible way to obtain hetero-structure photocatalyst with high activity because  $\text{KTaO}_3$  was considered as a stable photocatalysis.

Recently, application of photocatalysis in waste water treatment have aroused research interest by using solar energy is also considered employing in further application. For example, p-nitrophenol, which can be produced as intermediate of dyes, medicines [23] and pesticides [24], has a strong irritating effect on human skin and can cause huge damage to liver if adsorbed by respiratory tract [25]. It is not readily degradable and thus considered to be a severe wastewater pollutant. Photodegradation is a promising approach to remove hazardous p-nitrophenol. It has been shown that  $\text{TiO}_2$  and  $\text{ZnO}$  can be used to photochemically degrade p-nitrophenol and its efficiency can be further enhanced by constructing heterostructures [25–28]. To our best knowledge, the photocatalytic behaviour of perovskite potassium tantalate ( $\text{KTaO}_3$ ) and its heterostructures on degradation of p-nitrophenol has not been studied. Herein, we report the in-situ growth of Au of  $\text{KTaO}_3$  sub-micron cubes via a facile wet-chemical approach. The prepared  $\text{KTaO}_3/\text{Au}$  hetero-nanocrystals exhibit enhanced photodegradation performance on p-nitrophenol compared with bare  $\text{KTaO}_3$  nanocrystals.

## 2. Materials and Methods

### 2.1. Chemicals and Reagents

Tantalum pentoxide ( $\text{Ta}_2\text{O}_5$ ) and gold chloride tetrahydrate ( $\text{HAuCl}_4 \cdot 4\text{H}_2\text{O}$ , 99%) were purchased from Aladdin Reagent Co., Ltd. (Shanghai, China). Potassium hydroxide (KOH), Sodium citrate and ascorbic acid (A.A.) were purchased from Alfa Aesar Co., Ltd. (Tianjin, China). Sodium borohydride ( $\text{NaBH}_4$ ) and p-nitrophenol were purchased from Sigma-Aldrich Co., Ltd. (Shanghai, China). All of chemicals and reagents in this work are of analytical grade and used without further purification.

### 2.2. Synthesis of $\text{KTaO}_3$ and $\text{KTaO}_3/\text{Au}$ Nanocrystals

$\text{KTaO}_3$  nanocrystals were synthesized via hydrothermal method. To be specific, for  $\text{KTaO}_3$ , 1 mmol of  $\text{Ta}_2\text{O}_5$  and 0.5 mol of KOH were mixed in 30 mL of water under continuous stirring for 1 h, followed by transferring into a 50 mL Teflon-lined stainless steel autoclave (Yalunda, Beijing, China) and heating at 160 °C for 16 h. After the autoclave was naturally cooled to room temperature, the sample was purified by centrifugation at 3000 rpm for 8 min and redispersed in water for several times. The final nanocrystals were dispersed in 20 mL water.

For fabrication of  $\text{KTaO}_3/\text{Au}$  heterostructures with different Au loadings, the obtained  $\text{KTaO}_3$  was dispersed into 10 mL water, and 0.5 mL (1.0 mL, or 10  $\mu\text{L}$ ) of  $\text{HAuCl}_4$  (0.48  $\text{mmol}\cdot\text{L}^{-1}$ ) and 0.1 mL ascorbic acid (0.1  $\text{mol}\cdot\text{L}^{-1}$ ) solution was separately added to the above colloid dispersion. The reaction solution was further stirred for 24 h at room temperature. The product was collected by centrifugation at 3000 rpm for 10 min to remove the self-nucleated Au nanoparticles. The raw product was further purified by centrifugation at 3000 rpm for 10 min and re-dispersed in water for several times and re-dispersed in 5 mL water.

Au nanoparticles were synthesized via hydrothermal method, 4 mL of 1% sodium citrate aqueous solution were mixed in 30 mL of water under stirring at 70 °C for 10 min. Then, 0.4 mL of  $\text{HAuCl}_4$  (0.48  $\text{mmol}\cdot\text{L}^{-1}$ ) was added to above mixed solution, the solution was continuously stirred at 70 °C, the reaction was stopped until the solution turned to wine red and naturally cooled to room temperature. The raw product was collected by centrifugation at 5000 rpm for 10 min and redispersed into water.

### 2.3. Characterization

X-ray diffraction (XRD) pattern of as-prepared samples was collected with a Bruker D8 X-ray diffractometer (Bruker, Billerica, MA, USA) with  $\text{Cu } \alpha$  (wavelength = 1.5406 Å). The scanning electronic microscopy (SEM, Carl Zeiss AG, Oberkochen, Germany) of as-prepared samples was conducted by using a ZEISS SUPRA@55 scanning electron microscope. The transmission electron microscopy (TEM, FEI, Hillsboro, OR, USA) images were collected on FEI T12 transmission electron microscope (working

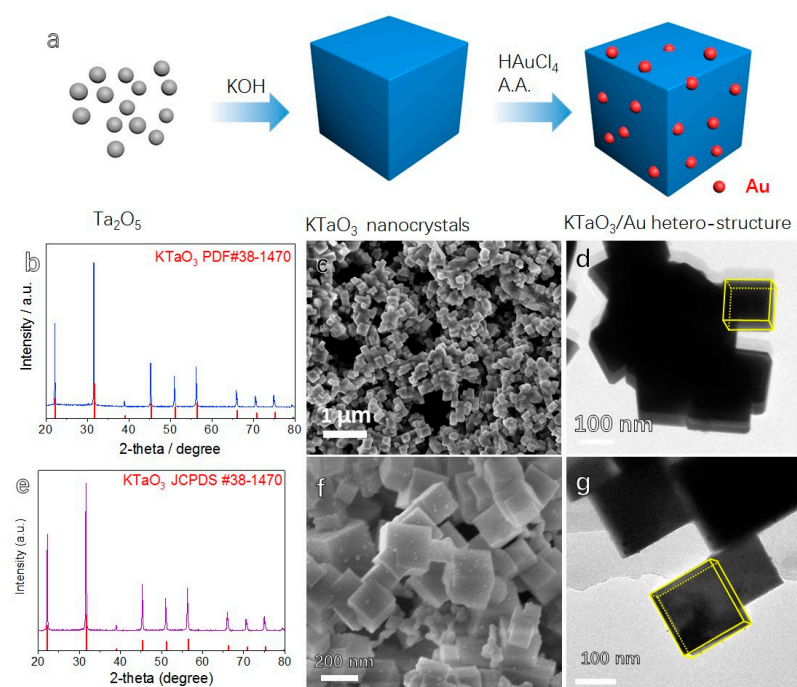
at 80 kV acceleration voltage). High resolution TEM (HRTEM) and element mapping analysis were performed on Tecnai G2 F30 transmission electron microscope (Thermo Fisher Scientific, Waltham, MA, USA). The UV-vis spectra were measured on UV-2600 (SHIMADZU, Kyoto, Japan).

#### 2.4. Photodegradation Measurement

KTaO<sub>3</sub> or KTaO<sub>3</sub>/Au nanocrystals (30.0 mg) were dispersed into 100 mL aqueous solution of 10 ppm p-nitrophenol and 2 ppm NaBH<sub>4</sub> by sonication for 30 min in the dark. The resulting suspension was continuously stirred under illumination of a Xe lamp with full radiation (including violet light and visual light, the wavelength range of radiation is 320–780 nm. Perfectlight, 300 W; the light power was 300 mW and the light power density was 400 mW/cm<sup>2</sup>). 4 mL aliquots were sampled every 60 min and centrifuged to remove catalyst particles. The collected solution was analysed with a UV-vis spectrometer. Au nanoparticles with UV-vis spectral equivalent concentration to KTaO<sub>3</sub>/Au heterostructures were used photodegradation measurement. The blank experiment is carried out without any catalyst, and the dark light experiment is operated without irradiation, other operations are the same as above. The stability of KTaO<sub>3</sub>/Au for photodegradation was characterized by recycling the catalysts after photodegradation test for 1 h and dispersing the recycled catalysts into the fresh p-nitrophenol solution for another runs. The repeat characterizations were carried out 6 run.

### 3. Results and Discussion

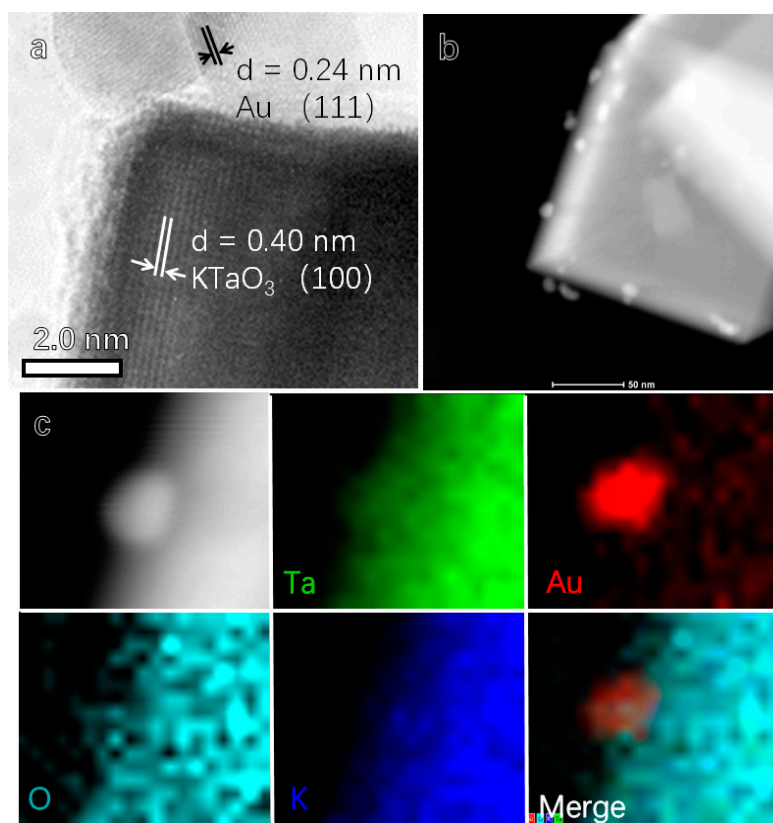
Figure 1a shows the schematic diagram of in-situ growth of Au nanoparticles on KTaO<sub>3</sub> sub-micron cubes which were prepared via a hydrothermal method in a relatively high concentration of KOH solution without surfactants. As shown in Figure 1b, hydrothermally processed KTaO<sub>3</sub> possess a cubic perovskite phase (JCPDS #38-1470) with good crystallinity. Figure 1c,d shows the SEM and TEM images of as-prepared KTaO<sub>3</sub> nanocrystals, indicating that sub-micron cubes KTaO<sub>3</sub> with an average size of ~200 nm have been obtained. Figure 1d shows the sharp edges of as-prepared KTaO<sub>3</sub> nanocrystals.



**Figure 1.** (a) Schematic of preparing of KTaO<sub>3</sub> sub-micron cubes and KTaO<sub>3</sub>/Au hetero-structure; (b) XRD patterns; (c) SEM images and (d) TEM images of as-prepared KTaO<sub>3</sub> nanocrystals; (e) XRD patterns; (f) SEM images and (g) TEM images of as-prepared KTaO<sub>3</sub>/Au heterostructure nanocrystals.

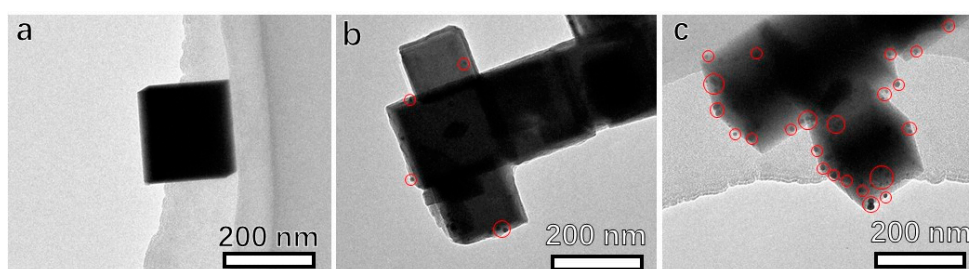
By mixing the as-prepared potassium tantalate nanocrystals with an appropriate concentration of  $\text{HAuCl}_4$  solution and ascorbic acid solution, in-situ growth of Au on  $\text{KTaO}_3$  sub-micron cubes can take place. As presented in Figure 1e, the XRD pattern confirms the presence of cubic  $\text{KTaO}_3$  phase, while the diffraction peaks of Au are too weak to be presented due to their small size. Furthermore, the XRD pattern of  $\text{KTaO}_3/\text{Au}$  hetero-structure confirmed that  $\text{KTaO}_3$  was stable during loading Au nanoparticles. The SEM image (Figure 1f) shows that the surface of cubic  $\text{KTaO}_3$  nanocrystals become rough because of the loading of Au nanocrystals. TEM image of (Figure 1g) cubic  $\text{KTaO}_3/\text{Au}$  indicates that the size of loaded Au nanoparticles is about 5 nm. It is also shown in Figure 1g that Au nanoparticles grow on the surface of the  $\text{KTaO}_3$  nanocrystals, which agrees with the rough surface of as-prepared products after Au loading observed in SEM images. In the reported methods for synthesis of  $\text{KTaO}_3$  based heterostructures, surfactants were usually employed [28,29]. In our case, Au was anchored and accumulated by  $\text{OH}^-$  on the surface of  $\text{KTaO}_3$ , and further grew into nanoparticles. Furthermore, the lattice mismatch between  $\text{KTaO}_3$  and Au is calculated (Table S1) and the largest mismatch is about 20%. The large strain on the interface between  $\text{KTaO}_3$  and Au prevent Au growing into a large particle and consequently, Au nanoparticles grown on the surface of  $\text{KTaO}_3$  will have small size.

Figure 2a presents the HRTEM image of  $\text{KTaO}_3/\text{Au}$  hetero-structure. The fringe distance of loaded nanoparticles was measured as 0.21 nm, which is consistent with the lattice spacing of (111) facets of Au. The fringe distance of the nanocube is 0.40 nm, in agreement with the lattice spacing of (100) facets of cubic  $\text{KTaO}_3$ . The HAADF-STEM (High-Angle Annular Dark Field) images (Figure 2b) clearly confirmed the loading of Au nanoparticles on the as-prepared  $\text{KTaO}_3$  nanocrystals. As shown in Figure 2c, the according element mapping shows that the elements of K, Ta and O distribute in the range of the  $\text{KTaO}_3$  nanocube while the Au element focuses on the zone of nanoparticles, which obviously illustrates the growth of Au nanoparticle on  $\text{KTaO}_3$  sub-micron cubes.



**Figure 2.** (a) HRTEM image, (b) HAADF-STEM image and (c) element mapping of as-prepared  $\text{KTaO}_3/\text{Au}$  hetero-structure.

The concentration of Au source plays an important role in controlling the in-situ growth of Au nanoparticles on  $\text{KTaO}_3$  sub-micron cubes. Figure 3 shows the TEM images of series of as-prepared  $\text{KTaO}_3/\text{Au}$  hetero-structure with different amount of  $\text{HAuCl}_4$  solution. By using  $0.005 \mu\text{mol}$  of  $\text{HAuCl}_4$  (Figure 3a), almost no Au nanoparticles could be found on the  $\text{KTaO}_3$  sub-micron cubes, and only very few Au nanoparticles with 10 nm of size were non-uniformly formed on the  $\text{KTaO}_3$  nanocrystal when the employed  $\text{HAuCl}_4$  amount increased to  $0.25 \mu\text{mol}$  (Figure 3b). As the  $\text{HAuCl}_4$  amount increased to  $0.5 \mu\text{mol}$ , the 5 nm of Au nanocrystals were found to be well dispersed on the  $\text{KTaO}_3$  nanocrystal. In-situ growth of Au on the surface of  $\text{KTaO}_3$  sub-micron cubes is a hetero nucleation process. Insufficient amount of  $\text{HAuCl}_4$  would not lead to the nucleation of Au. A proper concentration of  $\text{HAuCl}_4$  ensured that  $\text{Au}^{3+}$  was reduced and then nucleated on the surface of  $\text{KTaO}_3$  nanocrystal. On the other hand, if a substantial amount of  $\text{HAuCl}_4$  was reduced rapidly, self-nucleation rather than hetero-nucleation on the surface of  $\text{KTaO}_3$  would occur.



**Figure 3.** TEM images of series of as-prepared  $\text{KTaO}_3/\text{Au}$  hetero-structure with different amounts of  $\text{HAuCl}_4$ : (a)  $0.005 \mu\text{mol}$ ; (b)  $0.25 \mu\text{mol}$ ; (c)  $0.5 \mu\text{mol}$ .

The above results illustrate that Au nanocrystals are loaded onto the potassium tantalate nanocrystals by reducing  $\text{HAuCl}_4$  and well-defined hetero-structures were formed, which provide a possible way to study the Au enhancement on photocatalytic response. Figure 4a presents the diffuse reflection spectra of as-prepared potassium tantalate nanocrystals and potassium tantalates/Au hetero-nanostructures. As shown in Figure 4a, the main absorption of  $\text{KTaO}_3$  nanocrystals locates at ultraviolet zone ( $\lambda < 420 \text{ nm}$ ) and after Au loading, the as-prepared hetero-structures showed enhanced visible-light absorption. It is reported that the absorption range of Au nanoparticles is located at  $500\text{--}550 \text{ nm}$ , exhibiting red colour depending on their morphologies and sizes [30]. Therefore, the UV-vis spectrum of  $\text{KTaO}_3/\text{Au}$  with enhanced absorption peak of visible light at  $530 \text{ nm}$  should result from the Au nanoparticles loading. The diffuse reflection spectra showed that after loading Au nanoparticles, the bandgap and exists-hole were changed.

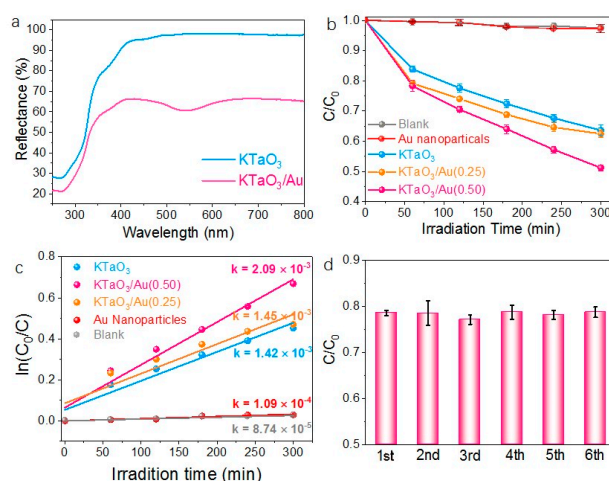


**Figure 4.** (a) UV-vis diffuse reflectance spectra of  $\text{KTaO}_3$  nanocrystals and  $\text{KTaO}_3/\text{Au}$  hetero-structure; (b,c) photocatalytic characterization, (d) the photodegradation processes run by replicate.

As shown in Figure S1, the p-nitrophenol with KTaO<sub>3</sub>/Au(0.5) was placed in dark condition and the result shows that little absorption of p-nitrophenol occurred on the surface of catalysts. The photodegradation curves are presented in Figure 4b, showing that KTaO<sub>3</sub>/Au nanocrystals have a higher degradation efficiency than KTaO<sub>3</sub> nanocrystals while little of p-nitrophenol photodegraded by using 10 nm of Au nanoparticles (Figure S2) or without using catalysts. As presented in Figure 4b, the blank case reveals that the p-nitrophenol was stable under UV-vis light irradiation and Au nanoparticle showed little capability on photodegradation of p-nitrophenol, which reveals that the capability of KTaO<sub>3</sub>/Au hetero-structure on photodegradation of p-nitrophenol arises from the synergetic effect of Au nanoparticles and KTaO<sub>3</sub>. Comparing the photodegradation of p-nitrophenol on KTaO<sub>3</sub>/Au with different Au loading, KTaO<sub>3</sub>/Au(0.5) exhibits higher activity than KTaO<sub>3</sub>/Au(0.25), which suggests that the more Au loading brings higher activity and confirms that the photodegradation enhancement results from Au loading. To have a better understanding of the kinetics, the photodegradation process of p-nitrophenol has been fitted to a pseudo-first-order reaction according to the following equation,

$$C = C_0 e^{-kt} \quad (1)$$

where  $C$  is the concentration of p-nitrophenol at time  $t$ ,  $C_0$  the initial concentration of p-nitrophenol, and  $k$  the reaction rate constant. Just shown in Figure 4b, Au nanoparticles exhibited little activity on degradation of p-nitrophenol and after loading Au, obviously higher activity was obtained on KTaO<sub>3</sub>/Au hetero-structures. Furthermore, the more Au loading resulted the higher activity. Figure 4c shows the fitted curves, in which the plots between  $\ln(C_0/C)$  and  $t$  are presented with  $k$  derived from the slope of the fitted linear curve according to Equation (1). The reaction rate constants ( $k$ ) are  $2.09 \times 10^{-3} \text{ min}^{-1}$  on KTaO<sub>3</sub>/Au and  $1.42 \times 10^{-3} \text{ min}^{-1}$  on KTaO<sub>3</sub> respectively. The  $k$  value is about 20 times as the case on Au nanoparticles or blank (Figure 4c). Furthermore, the  $k$  of KTaO<sub>3</sub>/Au(0.5) is obviously higher than KTaO<sub>3</sub>/Au(0.25) that is a bit higher than KTaO<sub>3</sub>. It is thus shown the photo-degradation efficiency of p-nitrophenol on KTaO<sub>3</sub> can be enhanced by forming hetero-structures with Au, due to the improved light absorption and charge separation. The photodegradation processes run by replicate of KTaO<sub>3</sub>/Au (Figure 4d) hetero-structure were carried out with irradiation for 60 min. The results showed that the activity of KTaO<sub>3</sub>/Au hetero-structure on remained well during photodegradation, which hinted that the KTaO<sub>3</sub>/Au hetero-structure was stable under UV-vis irradiation. Figure 4d showed the photodegradation of p-nitrophenol run by replicate and the results showed that the activity of the KTaO<sub>3</sub>/Au hetero-structure remain well during photodegradation of p-nitrophenol. Just present in Figure 4d, after 6 run of photocatalysis characterization the activity of KTaO<sub>3</sub>/Au hetero-structure remain well, which also hinted the stability of KTaO<sub>3</sub>/Au hetero-structure.

#### 4. Conclusions

In summary, in-situ growth of Au on KTaO<sub>3</sub> sub-micron cubes has been achieved by reducing H<sub>2</sub>AuCl<sub>4</sub> on the surface of hydrothermally-grown potassium tantalate nanocrystals. Loading of Au nanoparticles on KTaO<sub>3</sub> nanocrystals enriched KTaO<sub>3</sub> additional UV-vis absorption in the red light region. Both KTaO<sub>3</sub> and KTaO<sub>3</sub>/Au nanocrystals were shown to be active in the photo-degradation of p-nitrophenol while the loading of Au on KTaO<sub>3</sub> clearly improved the photo-degradation efficiency of p-nitrophenol compared to that on bare KTaO<sub>3</sub> nanocrystals. The comparison of p-nitrophenol photodegradation on KTaO<sub>3</sub>/Au (0.5) and KTaO<sub>3</sub>/Au (0.25) confirmed that the Au nanoparticles loading brings enhancement on photodegradation of p-nitrophenol.

**Supplementary Materials:** The following are available online at <http://www.mdpi.com/1996-1944/12/12/1950/s1>, Figure S1: The degradation curves of p-nitrophenol with KTaO<sub>3</sub>/Au(0.5) in dark condition, Figure S2: The TEM image of the single Au nanoparticles, Table S1: Lattice mismatches of KTaO<sub>3</sub> and Au nanoparticles.

**Author Contributions:** conceptualization, J.X., C.Z., B.L. and J.W.; methodology, S.C. and M.J.; Characterization, C.Y. and K.Z.; photodegradation, Q.D.

**Funding:** This work was supported by Technology Plan of Shenzhen City (Grant no. JCYJ20170412171554022), National Natural Science Foundation of China (Grant no. 51673117), the Science and Technology Innovation Commission of Shenzhen (Grant no. JCYJ20150529164656097, JSGG20160226201833790, JCYJ20170818093832350), Guangdong Natural Science Fund for Distinguished Young Scholars (Grant no. 2016A030306020) and Guangdong Youth Talent Plan (Grant no. 2015TQ01C536).

**Conflicts of Interest:** The authors declare no conflict of interest.

## References

1. Marchelek, M.; Bajorowicz, B.; Mazierski, P.; Cybula, A.; Klimczuk, T.; Winiarski, M.; Fijałkowska, N.; Zaleska, A. KTaO<sub>3</sub>-based nanocomposites for air treatment. *Catal. Today* **2015**, *252*, 47–53. [[CrossRef](#)]
2. Yucel, I.; Cakmak, S. Effect of oxygen vacancy on Sb<sup>3+</sup>, Nb<sup>3+</sup> and V<sup>3+</sup> doped KTaO<sub>3</sub> compounds. *Optik* **2019**, *178*, 467–477. [[CrossRef](#)]
3. Rossella, F.; Perucchini, L.; Galinetto, P.; Sarnoggia, G.; Mozzati, M.C.; Azzoni, C.B.; Badalyan, A.G.; Trepakov, V.A.; Syrnikov, P.P. Influence of Cu ions on the photo-transport properties in KTaO<sub>3</sub>: (Cu,V) single crystals. In *Physica Status Solidi C—Current Topics in Solid State Physics*; Stutzmann, M., Ed.; Wiley: Hoboken, NJ, USA, 2007; Volume 4, p. 1101.
4. Uniyal, M.; Bhatt, S.C.; Kashyap, S. Preparation and ultrasonic study of sodium potassium tantalate (Na<sub>1-x</sub>K<sub>x</sub>TaO<sub>3</sub>) mixed system. *Indian J. Pure Appl. Phys.* **2019**, *57*, 212–216.
5. Sudrajat, H.; Thushari, I.; Babel, S. Chemical state and coordination structure of La cations doped in KTaO<sub>3</sub> photocatalysts. *J. Phys. Chem. Solids* **2019**, *127*, 94–100. [[CrossRef](#)]
6. Marchena, C.L.; Pecchi, G.A.; Pierella, L.B. Selective styrene oxidation on alkaline tantalates ATaO<sub>3</sub> (A = Li, Na, K) as heterogeneous catalysts. *Catal. Commun.* **2019**, *119*, 28–32. [[CrossRef](#)]
7. Zhu, W.; Chao, J.-H.; Chen, C.-J.; Shang, A.; Lee, Y.G.; Yin, S.; Dubinskii, M.; Hoffman, R.C. Photon excitation enabled large aperture space-charge-controlled potassium tantalate niobate (KTN) beam deflector. *Appl. Phys. Lett.* **2018**, *112*, 132901. [[CrossRef](#)]
8. Hagiwara, H.; Higashi, K.; Watanabe, M.; Kakigi, R.; Ida, S.; Ishihara, T. Effect of Porphyrin Molecular Structure on Water Splitting Activity of a KTaO<sub>3</sub> Photocatalyst. *Catalysts* **2016**, *6*, 42–51. [[CrossRef](#)]
9. Shao, X.; Yin, X.; Wang, J. Nanoheterostructures of potassium tantalate and nickel oxide for photocatalytic reduction of carbon dioxide to methanol in isopropanol. *J. Colloid Interf. Sci.* **2018**, *512*, 466–473. [[CrossRef](#)]
10. Krukowska, A.; Winiarski, M.J.; Strychalska-Nowak, J.; Klimczuk, T.; Lisowski, W.; Mikołajczyk, A.; Pinto, H.P.; Puzyn, T.; Grzyb, T.; Zaleska-Medynska, A. Rare earth ions doped K<sub>2</sub>Ta<sub>2</sub>O<sub>6</sub> photocatalysts with enhanced UV-vis light activity. *Appl. Catal. B-Environ.* **2018**, *224*, 451–468. [[CrossRef](#)]
11. Rao, M.P.; Nandhini, V.P.; Wu, J.J.; Syed, A.; Ameen, F.; Anandan, S. Synthesis of N-doped potassium tantalate perovskite material for environmental applications. *J. Solid State Chem.* **2018**, *258*, 647–655. [[CrossRef](#)]
12. Huang, F.; Tian, H.; Meng, X.; Tan, P.; Cao, X.; Bai, Y.; Hu, C.; Zhou, Z. Large Room Temperature Electrocaloric Effect in KTa<sub>1-x</sub>Nb<sub>x</sub>O<sub>3</sub> Single Crystal. *Phys. Status Solidi-Rapid Res. Lett.* **2019**, *13*, 1800515. [[CrossRef](#)]
13. Yong, Z.; Ren, J.; Hu, H.; Li, P.; Ouyang, S.; Xu, H.; Wang, D. Synthesis, Characterization, and Photocatalytic Activity of g-C<sub>3</sub>N<sub>4</sub>/KTaO<sub>3</sub> Composites under Visible Light Irradiation. *J. Nanomater.* **2015**, *2015*, 1–7. [[CrossRef](#)]
14. Hu, S.; Liu, X.; Wang, C.; Camargo, P.H.C.; Wang, J. Tuning Thermal Catalytic Enhancement in Doped MnO<sub>2</sub>-Au Nano-Heterojunctions. *ACS Appl. Mater. Interf.* **2019**, *11*, 17444–17451. [[CrossRef](#)] [[PubMed](#)]
15. Chen, Z.; Xing, P.; Chen, P.; Chen, Q.; Wang, Y.; Yu, J.; He, Y. Synthesis of carbon doped KTaO<sub>3</sub> and its enhanced performance in photocatalytic H<sub>2</sub> generation. *Catal. Commun.* **2018**, *109*, 6–9. [[CrossRef](#)]
16. Reza Gholipour, M.; Dinh, C.-T.; Béland, F.; Do, T.-O. Nanocomposite heterojunctions as sunlight-driven photocatalysts for hydrogen production from water splitting. *Nanoscale* **2015**, *7*, 8187–8208. [[CrossRef](#)] [[PubMed](#)]
17. Wang, J.; Xiao, C.; Wu, X.; Zhang, G. Potassium Tantalate K<sub>6</sub>Ta<sub>10.8</sub>O<sub>30</sub> with Tungsten Bronze Structure and Its Photocatalytic Property. *Chin. J. Chem.* **2017**, *35*, 189–195. [[CrossRef](#)]
18. Wang, H.; Gao, Y.; Liu, J.; Li, X.; Ji, M.; Zhang, E.; Cheng, X.; Xu, M.; Liu, J.; Rong, H.; et al. Efficient Plasmonic Au/CdSe Nanodumbbell for Photoelectrochemical Hydrogen Generation beyond Visible Region. *Adv. Energy Mater.* **2019**, *9*, 1803889. [[CrossRef](#)]

19. Lin, S.; Lin, X.; Han, S.; Zhao, H.Y.; Hasi, W.; Wang, L. Highly monodisperse Au@Ag nanospheres: synthesis by controlled etching route and size-dependent SERS performance of their superlattices. *Nanotechnology* **2019**, *30*, 215601. [[CrossRef](#)]
20. Kumar, R.; Badilescu, S.; Packirisamy, M. Tuning of Morphology and Stability of Gold Nanostars Through pH Adjustment. *J. Nanosci. Nanotechnol.* **2019**, *19*, 4617–4622. [[CrossRef](#)]
21. Wang, Q.; Wang, Z.; Li, Z.; Xiao, J.; Shan, H.; Fang, Z.; Qi, L. Controlled growth and shape-directed self-assembly of gold nanoarrows. *Sci. Adv.* **2017**, *3*, e1701183. [[CrossRef](#)]
22. Wu, Y.; Cai, S.; Wang, D.; He, W.; Li, Y. Syntheses of water-soluble octahedral, truncated octahedral, and cubic Pt-Ni nanocrystals and their structure-activity study in model hydrogenation reactions. *J. Am. Chem. Soc.* **2012**, *134*, 8975–8981. [[CrossRef](#)]
23. Dej-Adisai, S.; Pitakbut, T. Determination of alpha-glucosidase inhibitory activity from selected Fabaceae plants. *Pak. J. Pharm. Sci.* **2015**, *28*, 1679–1683. [[PubMed](#)]
24. Wang, Z.P.; Ma, B.K.; Shen, C.; Cheong, L.Z. Direct, selective and ultrasensitive electrochemical biosensing of methyl parathion in vegetables using Burkholderia cepacia lipase@MOF nanofibers-based biosensor. *Talanta* **2019**, *197*, 356–362. [[CrossRef](#)] [[PubMed](#)]
25. Mishra, R.K.; Mohan, A.M.V.; Soto, F.; Chrostowski, R.; Wang, J. A microneedle biosensor for minimally-invasive transdermal detection of nerve agents. *Analyst* **2017**, *142*, 918–924. [[CrossRef](#)] [[PubMed](#)]
26. Lee, H.-G.; Sai-Anand, G.; Komathi, S.; Gopalan, A.I.; Kang, S.-W.; Lee, K.-P. Efficient visible-light-driven photocatalytic degradation of nitrophenol by using graphene-encapsulated TiO<sub>2</sub> nanowires. *J. Hazard. Mater.* **2015**, *283*, 400–409. [[CrossRef](#)] [[PubMed](#)]
27. Mou, H.; Song, C.; Zhou, Y.; Zhang, B.; Wang, D. Design and synthesis of porous Ag/ZnO nanosheets assemblies as super photocatalysts for enhanced visible-light degradation of 4-nitrophenol and hydrogen evolution. *Appl. Catal. B-Environ.* **2018**, *221*, 565–573. [[CrossRef](#)]
28. Naraginti, S.; Stephen, F.B.; Radhakrishnan, A.; Sivakumar, A. Zirconium and silver co-doped TiO<sub>2</sub> nanoparticles as visible light catalyst for reduction of 4-nitrophenol, degradation of methyl orange and methylene blue. *Spectrochim. Acta A* **2015**, *135*, 814–819. [[CrossRef](#)] [[PubMed](#)]
29. Bajorowicz, B.; Reszczyńska, J.; Lisowski, W.; Klimczuk, T.; Winiarski, M.; Słoma, M.; Zaleska-Medynska, A. Perovskite-type KTaO<sub>3</sub>-reduced graphene oxide hybrid with improved visible light photocatalytic activity. *RSC Adv.* **2015**, *5*, 91315–91325. [[CrossRef](#)]
30. Ji, M.W.; Xu, M.; Zhang, W.; Yang, Z.Z.; Huang, L.; Liu, J.J.; Zhang, Y.; Gu, L.; Yu, Y.X.; Hao, W.C.; et al. Structurally Well-Defined Au@Cu<sub>2-x</sub>S Core-Shell Nanocrystals for Improved Cancer Treatment Based on Enhanced Photothermal Efficiency. *Adv. Mater.* **2016**, *28*, 3094–3101. [[CrossRef](#)]



© 2019 by the authors. Licensee MDPI, Basel, Switzerland. This article is an open access article distributed under the terms and conditions of the Creative Commons Attribution (CC BY) license (<http://creativecommons.org/licenses/by/4.0/>).